



# Decreasing the environmental impact of carbon fibre production via microwave carbonisation enabled by self-assembled nanostructured coatings

Michał A. Stróżyk<sup>1</sup> · Muhammad Muddasar<sup>1</sup> · Timothy J. Conroy<sup>1</sup> · Frida Hermansson<sup>3</sup> · Matty Janssen<sup>3</sup> · Magdalena Svanström<sup>3</sup> · Erik Frank<sup>4</sup> · Mario Culebras<sup>5</sup> · Maurice N. Collins<sup>1,2</sup>

Received: 21 September 2023 / Revised: 6 February 2024 / Accepted: 12 February 2024 / Published online: 23 February 2024  
© The Author(s) 2024

## Abstract

The use of carbon fibre (CF)-based composites is of growing global importance due to their application in high-end sectors such as aerospace, automotive, construction, sports and leisure amongst others. However, their current high production cost, high carbon footprint and reduced production capability limit their use to high-performance and luxury applications. Approximately 50% of the total cost of CF production is due to the thermal conversion of polyacrylonitrile (PAN) precursor fibre (PF) to CF as it involves the use of high energy consumption and low heating efficiency in large furnaces. Looking at this scenario, this study proposes in the present study to use microwave (MW) heating to convert PF to CF. This is scientifically and technologically challenging since PF does not absorb microwave energy. While MW plasma has been utilised to carbonise fibres, it is the high temperature from the plasma that does the carbonisation and not the MW absorption of the fibres. Therefore, for the first time, this research shows how carbonisation temperatures of >1000 °C can be reached in a matter of seconds through the use of a novel microwave (MW) susceptor nanocoating methodology developed via a layer-by-layer assembly of multiwall carbon nanotubes (MWCNTs) on the PF surface. Remarkably, these CFs can be produced in an inexpensive domestic microwave and exhibit mechanical performance equivalent to CF produced using conventional heating. Additionally, this study provides a life cycle and environmental impact analysis which shows that MW heating reduces the energy demand and environmental impact of lignin-based CF production by up to 66.8% and 69.5%, respectively.

**Keywords** Carbon fibres · Layer-by-layer coating · MWCNTs · Susceptor coating · Microwave heating · LCA

## 1 Introduction

Carbon fibre-reinforced polymers (CFRP) are considered strategic materials for important sectors of our society (aeronautical, automotive and renewable energy) due to their advantageous properties such as high mechanical strength, lightweight and excellent chemical resistance [1–4]. However, their high cost, in terms of energy usage (about 14 times as energy intensive as producing steel) and carbon emissions, during production restricts their use to high-end applications where these production costs can be absorbed in the price of the final product. Therefore, the CF and composite industry is in urgent need of a destructive scientific solution that improves production efficiency and lowers the cost of CF.

This has gained further importance due to impending legislation and the worldwide green energy transition in which composite materials are crucial for the future development of wind turbine blades and lightweight electric vehicles [5,

✉ Maurice N. Collins  
maurice.collins@ul.ie

<sup>1</sup> School of Engineering, Bernal Institute, University of Limerick, Limerick, Ireland

<sup>2</sup> Advanced Materials and Bioengineering Research (AMBER) Centre, University of Limerick, Limerick, Ireland

<sup>3</sup> Division of Environmental Systems Analysis, Department of Technology Management and Economics, Chalmers University of Technology, Gothenburg SE-412 96, Sweden

<sup>4</sup> German Institutes for Textile and Fiber Research, Körchtalstrasse 26, 73770 Denkendorf, Germany

<sup>5</sup> Institute of Materials Science (ICMUV), University of Valencia, Paterna, Spain

6]. The high cost of CF is mainly attributed to the massive energy consumption during their production in particular during the conversion from PF to CF [7]. During CF production polyacrylonitrile (PAN) is wet spun into micrometre-size fibres that are thermally stabilised via crosslinking of PAN, and this allows shape retention during carbonisation where high temperatures of  $>1000$  °C are required to convert PAN into carbon. A similar process of stabilisation and carbonisation, although on a different scale, is employed for the synthesis of carbon nanofibres in order to maintain their shape [8, 9].

The composite industry has been searching for decades to overcome this cost problem. Currently, the most common approach is to replace PAN (representing the other 50% of the total cost) with cheaper biobased polymers such as lignin [8–10]. However, the mechanical performance of the CF obtained from these alternative precursors is much lower compared to the current PAN carbon fibres rendering them inadequate for many advanced applications including electromagnetic composites [11]. Therefore, this research presents a breakthrough sustainable manufacturing route that the composite industry requires to lower costs whilst maintaining exceptional mechanical performance. This disruptive new technology converts PF (PAN and lignin-based) utilising MW heating to CF. While microwave-assisted synthesis has previously been employed in the production of doped nanoparticles and graphene, its application in the creation of carbon fibres for the composite industry represents a groundbreaking innovation [12, 13]. This is particularly challenging since PAN and lignin PF do not absorb microwave energy. Therefore, this study has developed a methodology based on layer-by-layer coatings of colloidal suspensions of carbon-based MW susceptors.

The ability of a material to be heated in the presence of a MW field is defined by its dielectric loss tangent,  $\tan\delta = \epsilon''/\epsilon'$  [14]. Thus, MWCNTs are ideal as MW susceptors due to their high MW absorption and large aspect ratio for homogenous distribution on the PF surface at the nanoscale. For optimum MW heating, a moderate value of  $\epsilon'$  (real permittivity) should be combined with high values of  $\epsilon''$  (imaginary permittivity), to convert MW energy into thermal energy. MW heating offers a number of advantages over conventional heating such as (i) non-contact heating, (ii) energy transfer instead of heat transfer, (iii) rapid heating, (iv) selective heating, (v) volumetric heating, (vi) no inertia—of the MW power—(vii) heating from the PF surface and (viii) higher automation [15].

This manuscript presents a methodology for microwave heating to carbonise PF for the first time. This research provides a detailed study of showing how PAN and lignin precursor fibres can be converted to CF for high-end applications using a simple domestic MW oven. Moreover, this study provides a complete understanding of the process

involved during carbon fibre production utilising MW heating. The parameters used in the experiment were also verified with a MATLAB model of the MW heating process for PF in order to ensure consistency of results. The properties of the obtained CF are evaluated and compared with conventional CF using structural, mechanical and thermal characterisation. Finally, a full life cycle assessment is carried out to quantify the environmental and cost benefits of MW heating in CF production.

## 2 Experimental

### 2.1 Materials

Wet spun PAN fibres were obtained from Dralon GmbH, Germany. A blend of Alcell organosolv hardwood lignin (lignin) with a  $M_w = 3950$  g/mol, PDI = 4.7 (supplied by Tecnar, Ilsfeld, Germany) and thermoplastic polyurethane (TPU; Pearlthane ECO 12T95, obtained from Veltox, France, manufactured by Lubrizol) was developed at UL and prepared via melt-spinning into precursor fibre in a ratio of 50:50. Elicarb™ Multi-Walled Carbon Nanotubes (MWCNTs) with an average diameter of 10–12 nm were obtained from Thomas Swan and Co. Ltd. The following were purchased from Sigma-Aldrich (St. Louis, MI, USA): Poly(diallyldimethylammonium chloride) (PDADMAC), with a molecular weight of 100,000–200,000 g/mol, sodium deoxycholate (SDOC) ( $C_{24}H_{39}NaO_4$ ), tolylene-2,4-diisocyanate (TDI) and *n*-hexane.

### 2.2 Sample preparation

Prior to coating, the precursor fibre was corona-treated using an ETP BD-20AC Laboratory Corona Treater (Electro-Technic Products) to improve wettability. Precursor fibres were then coated with a microwave susceptor coating containing multi-walled carbon nanotubes (MWCNTs) [16]. The coating process involved preparing a cationic solution of 0.5 wt% PDADMAC in DI water and an anionic suspension of 0.05 wt% MWCNTs manually ground and dispersed in a 2 wt% SDOC aqueous solution. Fibres were immersed into a cationic solution for 5 min, followed by rinsing and drying using a gentle stream of compressed air, and then dipped into an anionic suspension for another 5 min. This process results in one deposition cycle of a susceptor coating, as illustrated in Fig. 1A. Immersion in PDADMAC solution deposits a layer of positively charged polymer on the precursor fibre surface. This is followed by immersion of the fibre in MWCNT aqueous suspension in SDOC. Electrostatic interaction between negatively charged SDOC and positively charged polymer leads to the deposition of MWCNTs. By repeating this procedure, a MWCNT-based thin film is grown incrementally with each cycle. After the

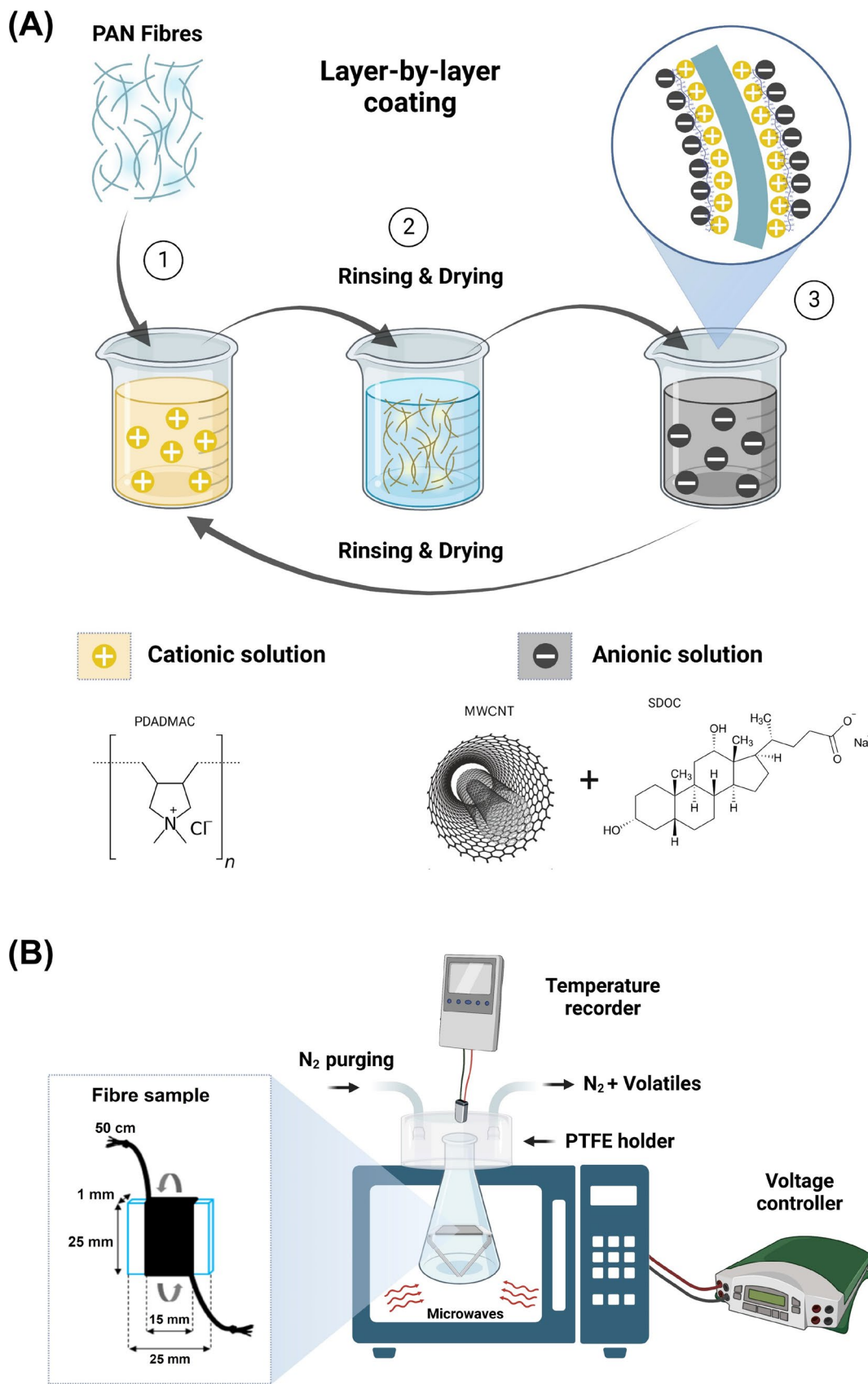


Fig. 1 A layer-by-layer cycle of susceptor coating deposition and B schematic representation of the microwave heating setup used in this study

initial cycle, all subsequent cycles were completed with 2 min dip times. This was repeated to deposit the desired number of susceptor layer cycles. Subsequent samples are referred to as  $Xc$ , where  $X$  signifies the number of cycles. Fibre samples with deposited multilayer films were air-dried overnight and then stored in a desiccator prior to further processing and characterisation. Two routes of sample preparation were investigated: (i) susceptor coatings before stabilisation and (ii) susceptor coatings after stabilisation.

### 2.3 Stabilisation

PAN samples were stabilised by heating in air at a ramp of  $1\text{ }^{\circ}\text{C min}^{-1}$  until  $250\text{ }^{\circ}\text{C}$ , followed by 1 h isothermal at  $250\text{ }^{\circ}\text{C}$ . Lignin/TPU blend samples were dipped for 5 min in a cross-linker solution of 10 wt% of tolylene-2,4-diisocyanate (2,4-TDI) in *n*-hexane following stabilisation in air at a ramp of  $1\text{ }^{\circ}\text{C min}^{-1}$  until  $250\text{ }^{\circ}\text{C}$ , with 2 h isothermals at 100, 150, 170, 200 and  $250\text{ }^{\circ}\text{C}$ .

### 2.4 Conventional carbonisation

Stabilised PAN and lignin/TPU fibres were placed on a stainless-steel holder inside a quartz tube reactor of an electrical LENTON tube furnace. The furnace was then closed and vented with  $\text{N}_2$  for 30 min. After that, samples were carbonised by heating to  $1000\text{ }^{\circ}\text{C}$  at  $10\text{ }^{\circ}\text{C min}^{-1}$  with a 30 min isothermal at  $1000\text{ }^{\circ}\text{C}$ .

### 2.5 MW heating

Fibres were wrapped around a quartz microscope slide and placed in a flask inside a microwave oven, as illustrated in Fig. 1B.  $\text{N}_2$  gas was allowed to flow through the flask for 30 min after insertion of the sample and during the heating. Microwave heating was performed in a modified domestic microwave with a maximum output power of 700 W. The microwave was operated in two modes: (a) full power and (b) progressive power levels. In mode (b), the voltage was increased incrementally from 160–165 V to provide five progressive levels of MW power, with the final one at 230 V (700 W). The power was unchanged until the sample temperature was stable, which resulted in differences in carbonisation times of progressive carbonisation runs. Total heating time was up to 20 min for mode (a) and 30–40 min for mode (b). MW carbonisation heating profiles were recorded using an IR pyrometer Calex PyroUSB PUA8 with a temperature range of 0– $1000\text{ }^{\circ}\text{C}$  or Optris CT 3 M with a temperature range of 250– $1800\text{ }^{\circ}\text{C}$ . Following experimental estimation which was in agreement with values found in the literature [17, 18], the emissivity was assumed to be constant at 0.9. After heating, the fibre was allowed to cool down to  $250\text{ }^{\circ}\text{C}$  in an  $\text{N}_2$  atmosphere prior to storage and characterisation.

Periodic signal noise/vibration was present in some of the recorded heating profiles, which is due to the periodical change of the electromagnetic field of the microwave [19]. These profiles were smoothed for clarity in Origin software.

### 2.6 Characterisation

SEM was performed utilising a Hitachi TM1000 at 15 kV for general imaging of the produced CF and a Hitachi SU70 microscope at 10 kV for higher magnification imaging. RAMAN spectra were recorded by utilising a Horiba LabRAM 1A spectrometer in a backscattering configuration, equipped with a 514.5 nm laser source, calibrated with the spectra of a silicon sample before each session. Fits of the spectra were obtained using a Pseudo-Voigt function in Origin software. The graphite particle size ( $L_a$ ) was calculated using a Tuinstra and Koenig proportionality improved by Cançado et al. for any laser in the visible range [20, 21]. Thermo-gravimetric analysis (TGA) was performed using a Setaram Labsys DSC-TGA in  $\text{N}_2$  atmosphere at a rate of  $10\text{--}20\text{ }^{\circ}\text{C/min}$  to  $1000\text{ }^{\circ}\text{C}$  and then held for a 5 min isothermal. Tensile testing of fibre samples was performed on the FAVIMAT single-fibre tester, using a clamping length of 12 mm and a speed of 0.5 and 1 mm/min for PAN and lignin/TPU samples, respectively. Measurements were carried out at DITF in Denkendorf, Germany. The results were analysed using one-way analysis of variance (ANOVA) and Tukey's test in order to determine their statistical significance. The  $p$ -value of  $< 0.05$  was considered statistically significant. A detailed description of the characterization procedure can be found in the Supporting Information.

### 2.7 Coupled electromagnetic-heat transfer model

MW heating of PF using susceptor technology was modelled in MATLAB. In order to model the transient temperature distribution on the precursor cross-section, it was necessary to couple the electromagnetic and heat transfer domains. MW heating was assumed to proceed mainly through conduction loss. For a more detailed description of assumptions and equations, the reader is referred to the Supporting Information.

### 2.8 LCA methodology

The life cycle analysis modelling was performed in OpenLCA, using CML2001, ecoinvent 3.3 [22] and ELCD (European Platform on Life Cycle Assessment) methodologies and databases. Data collected within the LIBRE project (Grant agreement ID: 720707) was used for lignin/TPU CF. For a more detailed description of assumptions, the reader is referred to the Supporting Information.

### 3 Results and discussion

MW carbonisation was applied for PAN PF, currently the most common precursor material for CF production. In order to find the optimum carbonisation methodology, PAN fibres were carbonised via MW heating utilising the full power mode and controlling the MW power in several steps.

PAN precursor fibres were coated with 1–5 c (cycles) of the susceptor, and the layer was applied before or after stabilisation. The coatings show a good degree of homogeneity, and the susceptors were well distributed along the precursor fibres (Fig. S9). SEM images, mechanical properties and carbonisation profiles of CFs produced via full-power MW carbonisation from PAN precursor are shown in Fig. 2. Cross-sections of CFs show characteristics of brittle fracture (Fig. 2A). In this case, oval pores/defects of up to about 1.5  $\mu\text{m}$  in the longest (radial) direction are observed in all samples. Pores are found along the circumference of the fibre's cross-section and sometimes elongated radially. Similar features were reported previously by Barnet and Norr in a structural model of high-modulus PAN-based CF [23, 24]. It was proposed that a radial structure of disordered crystalline webs and large voids is surrounded by highly ordered crystalline skin/sheath. Formation of such a structure was attributed to radial stresses and differential shrinkage during carbonisation and cooling of the fibre. These defects/voids visible in fibres are most likely caused by the high heating rates observed during MW carbonisation. Development of a skin-core structure could lead to stress between the two zones during shrinkage. It was previously reported that incomplete stabilisation could result in different orientations of the inner and outer zones of the cross-section [25]. Also, fast carbonisation leads to the evolution of large amounts of decomposition products over short periods of time instead of the slow diffusion of volatiles to the outer surface. This promotes the creation of relatively large voids. In general, voids in cross-sections are slightly smaller in CFs coated before stabilisation, due to lower  $T_{\text{max}}$  temperatures. Pores observed in CF produced via conventional carbonisation are much smaller and scarce, which suggests that the rates of heating or cooling have a predominant effect on their formation.

Mechanical properties of CFs produced via high-power MW carbonisation from PAN precursor are shown in Fig. 2B, C. Average tensile strength (TS), Young's moduli (YM) and strain of samples coated before stabilisation are in the range of 0.84–0.93 GPa, 75.5–160.7 GPa and 0.6–1.25%, respectively. Average TS, YM and strain of samples coated after stabilisation are in the range of 0.41–0.83 GPa, 76.5–131.75 GPa and 0.64–0.84%, respectively. The properties were benchmarked off the control sample, carbonised in a conventional tube furnace (Conv). Measured TS of 1.42 GPa, YM of 114.8 GPa and strain of 1.24% are close

to values previously reported for PAN carbonised with no tension control [26]. TS is generally slightly lower compared to the control, which can be attributed to premature fracture due to pores observed through SEM. Defects formed by thermal decomposition products are known to have a detrimental effect on mechanical properties during carbonisation at high heating rates [24]. However, overlapping of the error bars indicates that it was possible to produce CF with properties comparable to control CF (Conv). These promising results are supported by YM values which match those of the control. Microwaved fibres generally ruptured at strain values lower than that of the control, but an overlap of the error bars is also visible in this case. Coating before stabilisation produced CFs with higher TS, YM and strain. This can be explained by milder processing conditions (lower  $T_{\text{max}}$ ) during carbonisation. Also, highest values of TS and YM in both groups correspond to median values of  $T_{\text{max}}$ , which indicates improvement of mechanical properties when over-heating, and therefore, porosity is limited.

Heating profiles for full-power MW carbonisation of PAN precursor are shown in Fig. 2D, E. For clarity purposes, only the first 10 min of heating is presented. The samples experience extremely fast heating to temperatures above 800  $^{\circ}\text{C}$  in the first 30 s. Recorded maximum temperatures ( $T_{\text{max}}$ ) are in the range of 847–956  $^{\circ}\text{C}$  for fibres coated before stabilisation and 911–1076  $^{\circ}\text{C}$  for fibres coated after stabilisation. In general, the  $T_{\text{max}}$  increases with the increasing number of coating cycles and is higher for fibres coated after stabilisation. Coatings applied before stabilisation undergo degradation/melting during the stabilisation step (Fig. S8), which results in a decrease of the MW heating response. On the contrary, coatings applied after stabilisation respond efficiently to electromagnetic waves, most likely through increased electrical conductivity. It is also more fragile, more readily peeled off by the volatile matter, i.e. crosslinking condensation, dehydrogenation and denitrogenation reactions [24, 27], during carbonisation which presumably is the cause of the abrupt changes of recorded temperatures during MW heating, see Fig. S2. [28], Alternatively, some of the most abrupt peaks could be attributed to plasma formation [29].

Carbonisation conditions and properties of CFs produced via full-power MW carbonisation from PAN precursor are summarised in Table S2 and compared to conventional carbonisation at 1000  $^{\circ}\text{C}$ . Conversion rates are calculated from TGA curves and are in the range of 86–91% for CFs coated before stabilisation and 95–98% for CF coated after stabilisation (Fig. S3). This is in agreement with higher  $T_{\text{max}}$  temperatures recorded for samples coated after stabilisation, which results in fuller conversion to CF. The calculated graphitic crystallite size ( $L_a$ ) is in the range of 6.42–9.23 nm for CFs coated before stabilisation, 5.12–11.43 nm for CFs

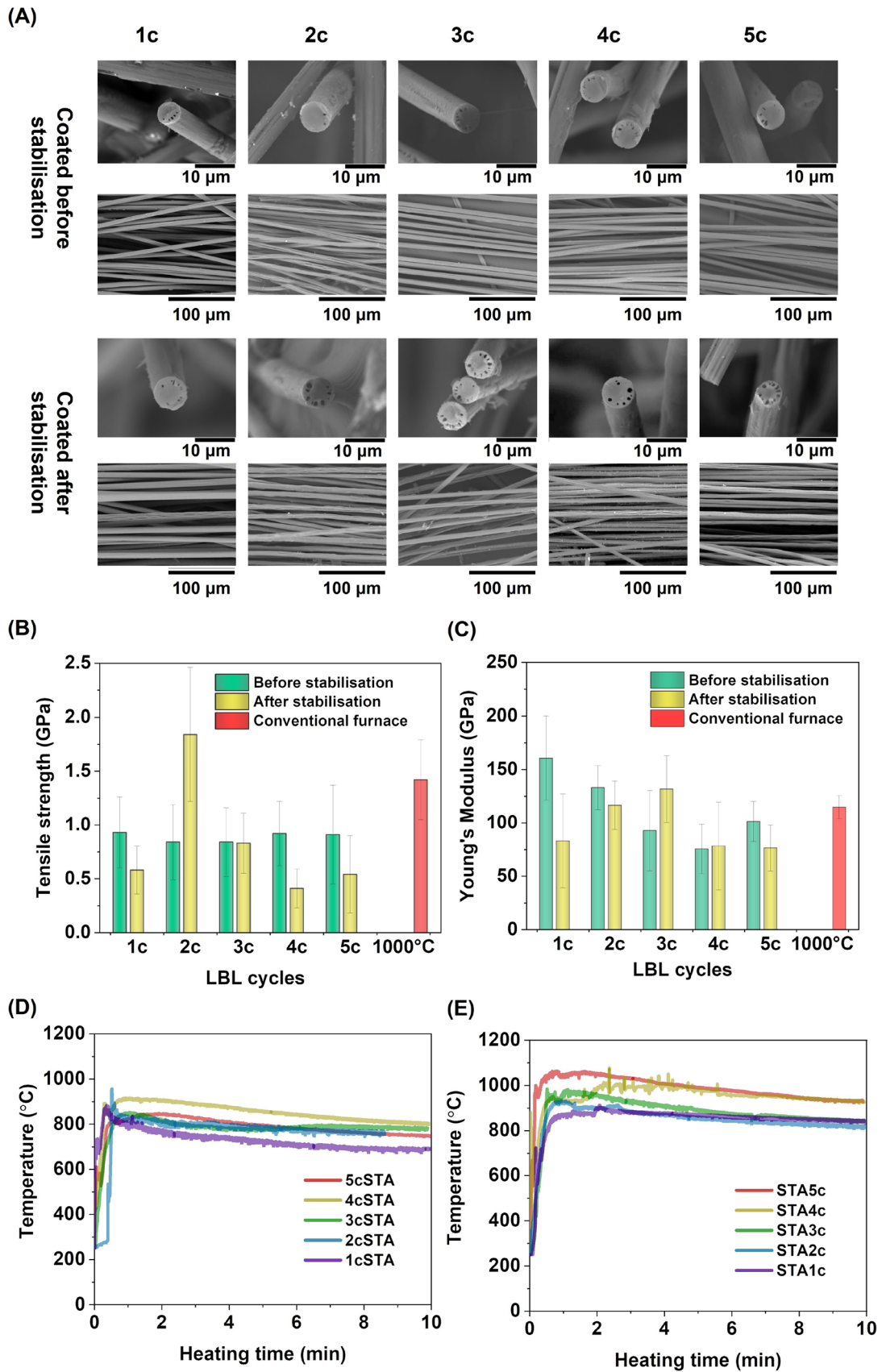


**Fig. 2** A SEM images of CFs produced via full-power MW carbonisation from PAN precursors, B, C mechanical properties of CFs and carbonisation temperature profiles of CFs coated D before and E after stabilisation

coated after stabilisation and 9.61 nm for sample carbonised conventionally (Conv). Crystallite size is generally larger at higher  $T_{\max}$ . CFs that reached temperatures close to or exceeding 1000 °C display crystallite sizes comparable with conventional carbonisation at 1000 °C. This is attributed to increased crystallite growth as the temperature or the duration of heat treatment is increased [30]. Generally, heat treatment at higher temperatures increases  $L_a$ , and this improves mechanical properties. Results show that the carbon phase of MW-heated CF is within range to produce mechanically viable CF; however, there is a disagreement between  $L_a$  and mechanical data (especially TS) for the MW-heated CF, and this strongly suggests that the elimination of defects is the main factor to optimise the performance of CFs produced by this new MW method.

For the case of the MW heating under progressive power levels, an equivalent batch of samples was prepared with the objective of preventing defects and improving the mechanical properties of the CFs produced via MW carbonisation. Heating profiles of an equivalent set of PAN samples carbonised at progressive power levels are shown in Figs. 3A, B and S4. Noticeably lower heating rates are observed during the initial stage at the lowest power, with temperatures not exceeding 600 °C in the first minutes of carbonisation. Increasing the MW power increases the rate of heating significantly and heats the samples to temperatures above 600 °C. The final stage at full power (230 V, 700 W) results in the highest heating rates and  $T_{\max}$  temperatures in the range of 690–827 °C for fibres coated before stabilisation and 695–974 °C for fibres coated after stabilisation.

SEM images of CFs produced via progressive MW carbonisation from PAN precursor are shown in Fig. 3C. Cross-sections show characteristics of brittle fracture. There were a very limited number of oval pores/defects in the fibres utilising this carbonisation protocol. In addition, the morphology of the pores found was shorter, narrower and sometimes needle-shaped. This can be explained by lower heating rates during the initial stages of heating and also lower  $T_{\max}$  compared to counterparts carbonised at full power only, which limits radial residual stress in the fibre and the development of cavities. Furthermore, milder carbonisation conditions lead to slower evolution of volatiles during MW heating and restrict the damage to the produced CF. Generally, it is possible to find similar amounts of defect-free cross-sections within both sample groups.

Mechanical properties of CFs produced via progressive MW carbonisation from PAN precursor are shown in Fig. 3D. Average TS, YM and strain of samples coated before

stabilisation are in the range of 0.42–0.88 GPa, 60.73–82 GPa and 0.56–1.26%, respectively. Average TS, YM and strain of samples coated after stabilisation are in the range of 0.23–1.18 GPa, 43–100 GPa and 0.34–1.31%, respectively. The results indicate that for this heating protocol, the optimum samples were achieved for the fibres coated with 5 cycles and carbonised after stabilisation which reached values very close to the control sample carbonised utilising conventional heating.

Carbonisation conditions and properties of CFs produced via progressive MW carbonisation from PAN precursor are summarised in Table S3 and compared to conventional carbonisation at 1000 °C. Conversion rate evaluated from TGA is in the range of 80.9–86.6% for fibres coated before stabilisation and 81–91.1% for fibres coated after stabilisation (Fig. S5). Conversion rate is lower compared to fibres carbonised at full power only. Incomplete carbonisation is in agreement with lower  $T_{\max}$  temperatures observed during progressive heating. The calculated graphitic crystallite size ( $L_a$ ) is in the range of 4.65–6.75 nm for CFs coated before stabilisation and 4.25–7.78 nm for CFs coated after stabilisation. The values are lower than  $L_a$  of their counterparts, which is in agreement with lower  $T_{\max}$  and results in a lower degree of orientation in CFs. Figs. S10 and S11 Raman spectra show clearly the D and G bands indicating the presence of a carbon phase in the MW-heated precursors.

A blend of lignin and polyurethane (50:50, lignin/TPU) was recently developed and identified as a promising precursor for CF production [31]. Melt-spun lignin/TPU precursor fibres were coated with MW susceptor to enable achievement of carbonisation temperatures during MW heating and conversion of sustainable lignin/TPU precursor into CF.

Firstly, full-power MW carbonisation was used to convert lignin-based fibres coated after stabilisation. Heating profiles of full-power MW carbonisation of lignin-based precursor are shown in Fig. 4A. Most of the samples experienced extremely fast heating to temperatures close to their  $T_{\max}$  in the first 15 s of MW heating. This was followed by a sudden drop to 300–500 °C and a subsequent rise to a stable temperature between 400 and 950 °C. Minor signal disruptions are observed (especially at higher temperatures), which are attributed to carbonisation reactions and the evolution of volatiles. Recorded  $T_{\max}$  are in the range of 500–1044 °C. Rates and maximum temperatures are observed to be more dependent on the number of susceptor coating cycles compared to MW heating of PAN. This can be attributed to the larger diameter of lignin-based fibres (~100 vs. ~10 µm). This leads to a smaller surface area covered by MW susceptor coating and a smaller number of individual fibres mounted for MW carbonisation. Consequently, there is less MW susceptor present during the heating of lignin/TPU compared to PAN carbonisation, which results in the enhancement of differences between cycles of susceptor coating and should enable easier optimisation of the MW heating.

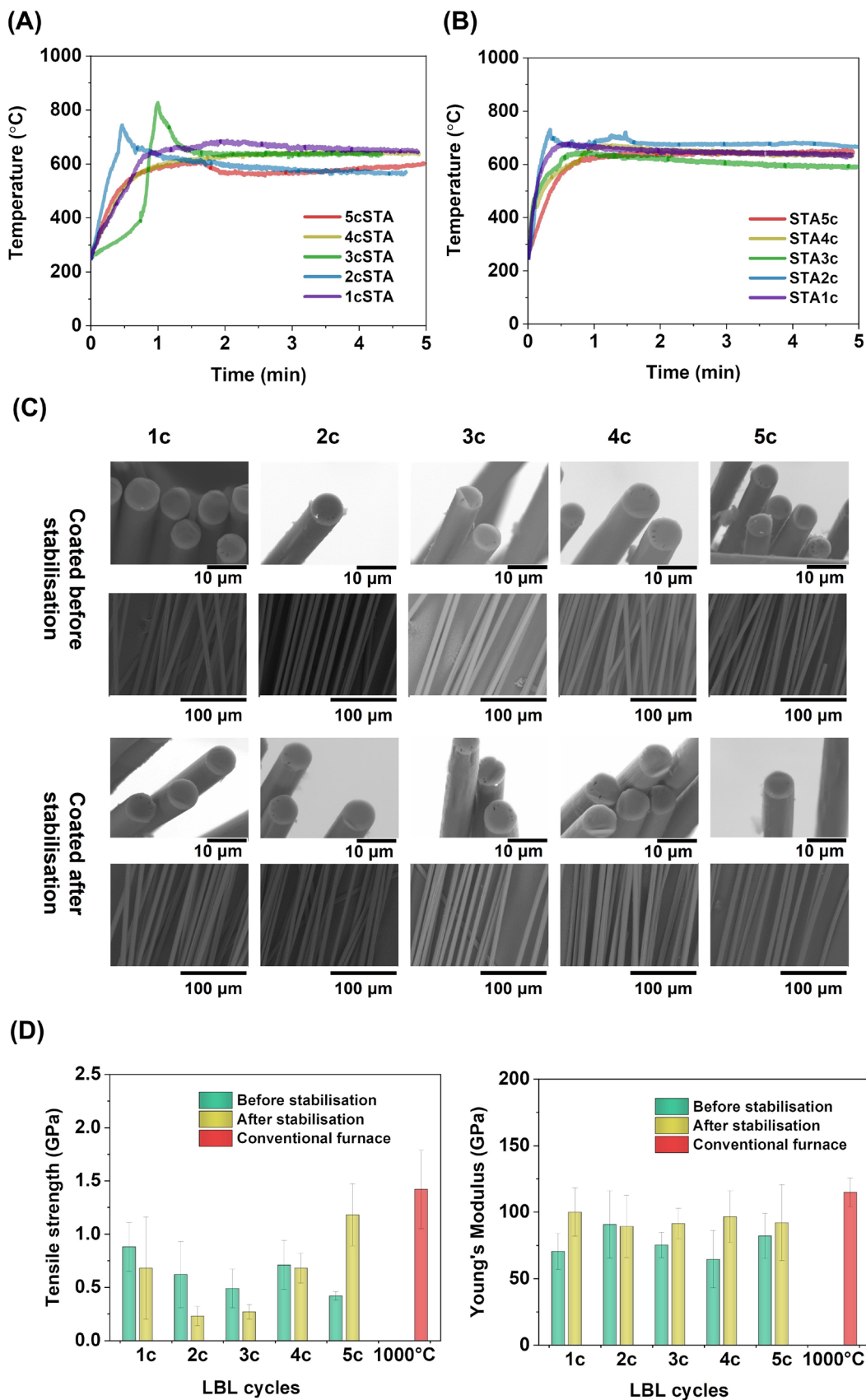




**Fig. 3** Heating profiles of CFs produced via progressive MW carbonisation from PAN precursor @ 175 V **A** before and **B** after stabilisation, **C** their SEM images and **D** mechanical properties

SEM images of CFs produced via full-power MW carbonisation from the lignin-based precursor are shown in Fig. 4B. Cross-sections show a brittle fracture of the fibres with highly porous structures observed for samples with 2 or more layers of susceptor coating. Porous cross-sections present a structure of interconnected pores (mostly oval pores with a diameter of up to about 20  $\mu\text{m}$  in the longer dimension and some long cavities and cracks with lengths of up to about 50  $\mu\text{m}$ ) surrounded by a sheath/skin with a thickness of up to 3  $\mu\text{m}$ . The skin-core structure could be predefined during stabilisation [32, 33], and this is enhanced for fibres with larger diameters due to incomplete stabilisation [34].

Smooth and homogeneous cross-sections of samples 1c and Conv (conventional carbonisation at 1000  $^{\circ}\text{C}$ ) suggest the following: (i) the porosity is induced at temperatures above  $T_{\text{max}}$  (1c) = 500  $^{\circ}\text{C}$  and (ii) it is most likely caused by extremely fast heating (up to 200  $^{\circ}\text{C s}^{-1}$  vs. 10  $^{\circ}\text{C min}^{-1}$  for Conv). Most likely, the formation of these pores in lignin-based CFs can be attributed to the release of volatiles during carbonisation [35, 36], gasification of oxygen [37]. High heating rate leads to a fast release of volatiles and highly porous morphology. In fact, the evolution of volatile solvents from the fibre can be used to prepare porous fibres via electrospinning [38]. Open pores and waviness of the outer surface are also observed for samples with two or more layers of susceptor coating. This is due to the porosity induced during carbonisation, which manifests itself in the form of open pores and distorted shapes of produced CFs. This is

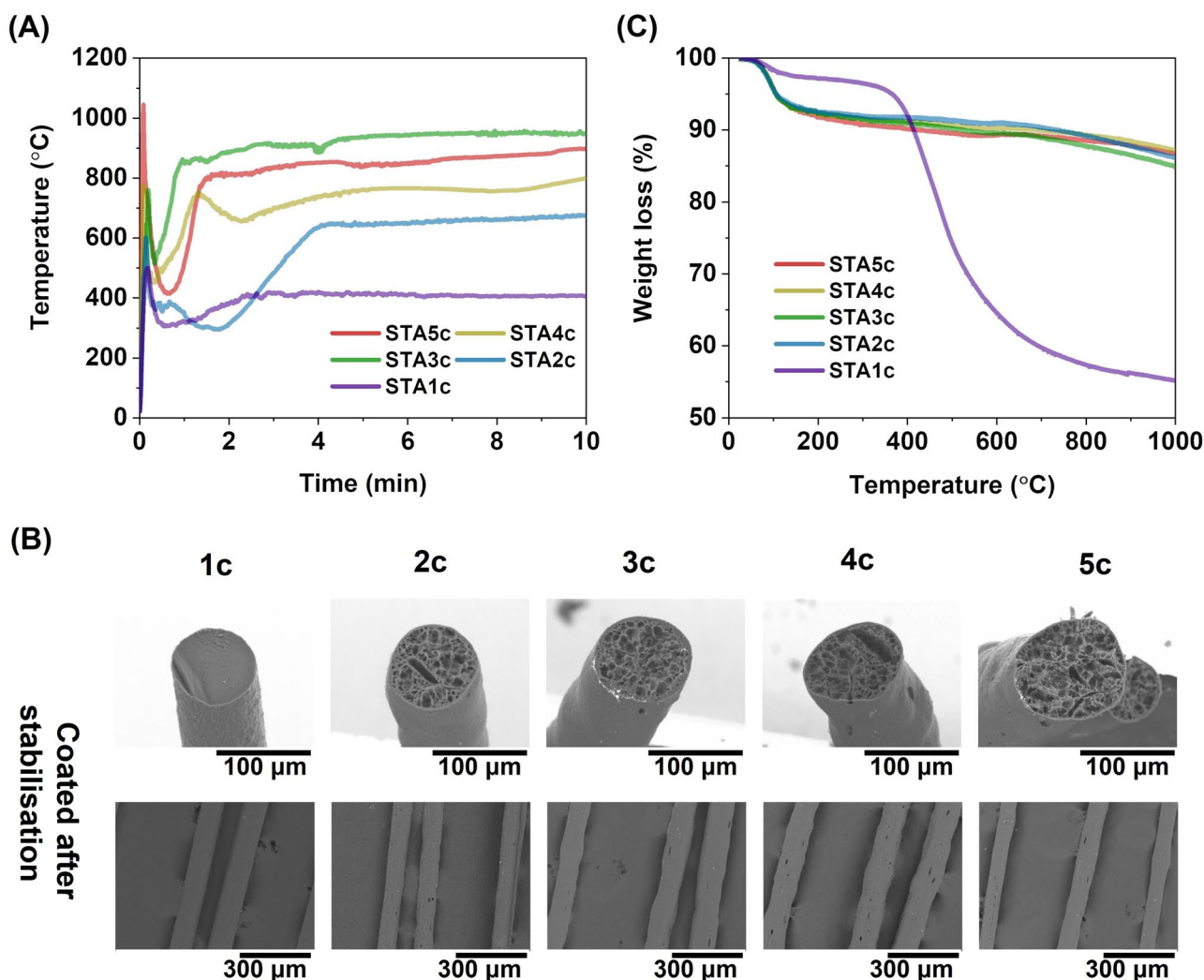


**Fig. 4** **A** Carbonisation temperature profiles, **B** TGA results and **C** SEM images of CFs produced via full-power MW carbonisation from lignin/TPU precursor

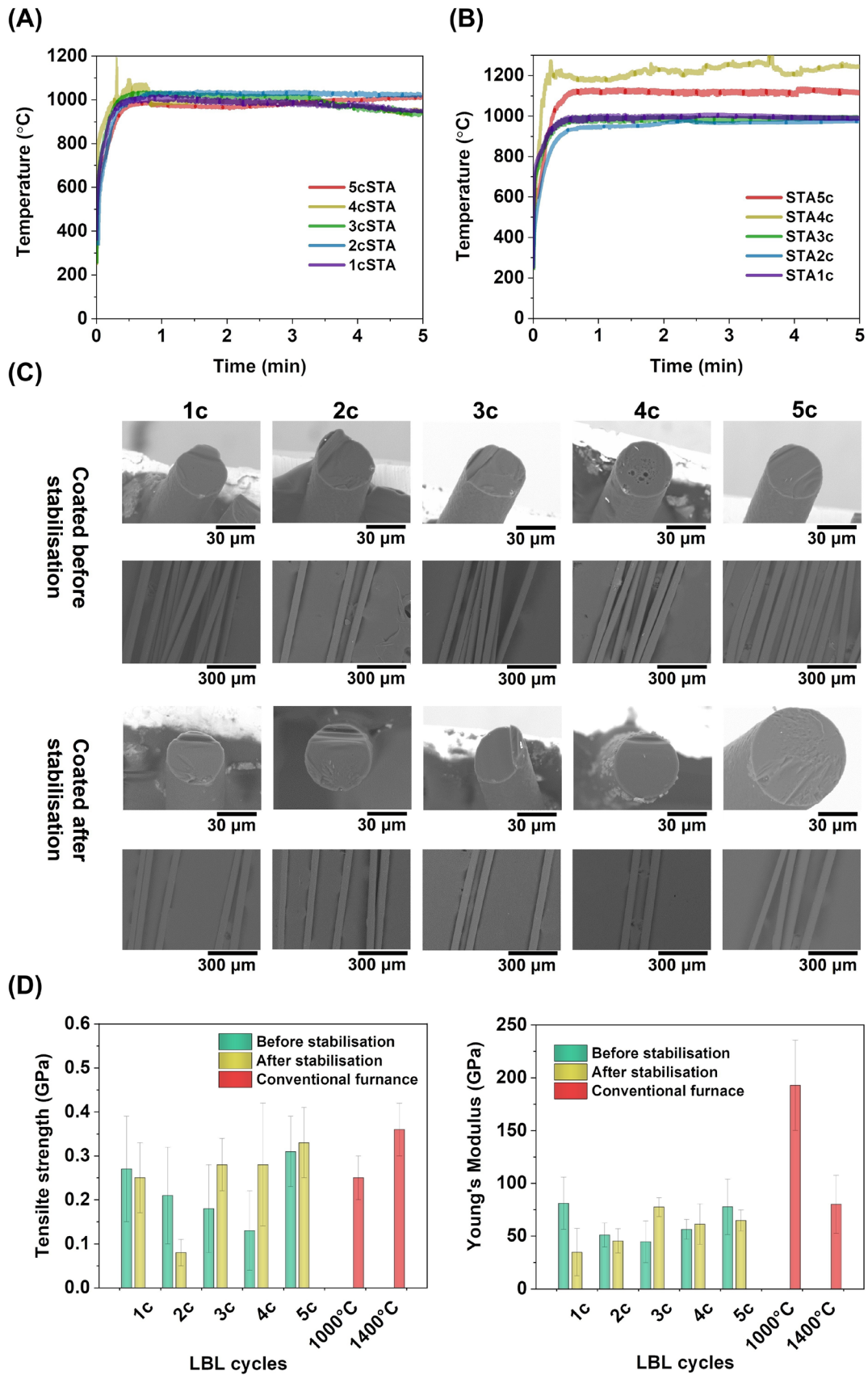


**Fig. 5** Heating profiles of CFs produced via progressive MW carbonisation from lignin/TPU precursor @ 230 V **A** before and **B** after stabilisation, **C** their SEM images and **D** mechanical properties

confirmed by previous reports, where prolonged heating at higher temperatures leads to the destruction of walls between pores and their appearance on the surface [39]. Samples 1c and Conv remain straight after the heat treatment. CFs presented here are too brittle for testing of mechanical properties due to the porosity observed through SEM.

Carbonisation conditions and properties of CFs produced via full-power MW carbonisation from the lignin-based precursor are summarised in Table S4 and compared to conventional carbonisation at 1000 °C. Conversion rate evaluated from TGA is in the range of 84.7–87% for samples 2–5c (Fig. 4C). The low yield of sample 1c (55%) can be attributed to the lowest  $T_{\max}$  reached by the fibre during MW heating (500 °C), which was not sufficient for carbonisation of the fibre. The lack of porosity on SEM images of this sample confirms that it was not exposed to conditions, experienced by the rest of the group. This also suggests that the pores observed in other samples were mostly formed at temperatures above 500 °C. The calculated graphitic crystallite size ( $L_a$ ) for samples 2–5c is in the range of 5.32–6.24 nm compared to 6.71 nm for sample Conv (conventional at 1000 °C). This is in consensus with  $T_{\max}$  temperatures and analogous to findings reported for PAN, where most of the samples have smaller  $L_a$  compared to Conv, due to  $T_{\max} < 1000$  °C. Although it is possible to calculate the  $L_a$  value (6.58 nm) for sample 1c, it is only theoretical. The sample is not fully carbonised, as suggested by TGA and the low intensity of the Raman spectrum. Furthermore, the method used here for  $L_a$  calculation applies only to crystallite size  $> 2$  nm. Raman spectra for lignin precursors are shown in Fig. S12 [21, 30].

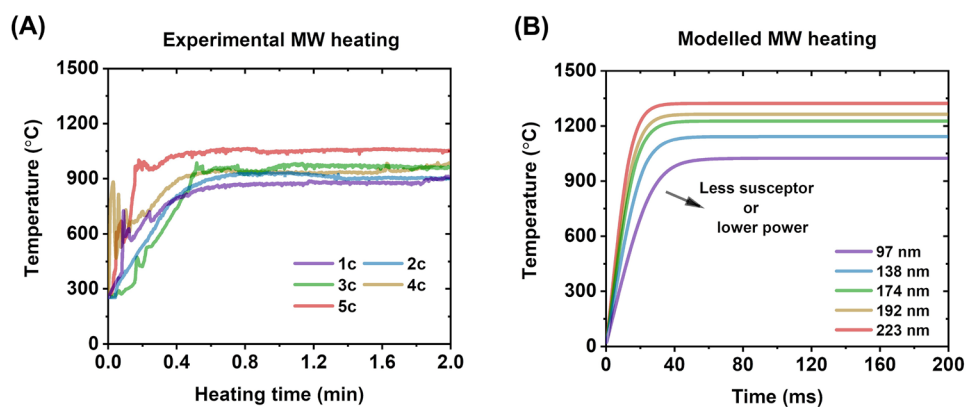
Progressive MW carbonisation was used to convert a set of lignin-based fibres coated with the MW susceptor before and after stabilisation, in order to find optimum conditions and improve the mechanical performance of CFs produced from this precursor. Heating profiles of lignin-based precursor samples carbonised at progressive power levels are shown in Figs. 5A, B and S6. Noticeably lower heating rates are observed during the initial stage at the lowest power. After 5 min of heating, most of the samples reach a temperature between 300 and 450 °C, which is usually higher for samples coated after stabilisation. This correlates with improved MW absorption observed previously for the susceptor layer prepared via this sequence. Increasing the MW power increases the rate of heating significantly. It is observed that at a certain point during the initial and intermediate stages of heating, sample temperature suddenly increases from about 400 °C to about 600–800 °C at which it tends to stabilise again. This sudden rise is recorded earlier in the process for samples with thicker susceptor coating.

Reduction of the heating rate before this transition is probably the key to process optimisation, as suggested by similar practice for conventional carbonisation of other hardwood lignin fibres [33]. After this, a relatively stable reading of temperature (sometimes preceded by a sharp peak instead of a round shoulder) is recorded and the temperature scales with MW power until the final stage at 230 V, 700 W. Recorded  $T_{\max}$  are in the range of 1020–1259 °C for fibres coated before stabilisation and 1000–1346 °C for fibres coated after stabilisation. Highest temperatures are recorded for samples after 4 cycles of susceptor coating (4c). Wider range and higher  $T_{\max}$  are observed for samples coated after stabilisation, which could be explained by improved MW absorption of these samples. It is important to note that the heating was not effective in samples without the susceptor coating since the PF fibres (PAN and lignin) were transparent to MW radiation (Fig. S14).

SEM images and mechanical properties of CFs produced via progressive MW carbonisation from the lignin-based precursor are shown in Fig. 5C. Cross-sections of CFs present evidence of brittle fracture. Most samples are defect-free with a smooth and homogeneous morphology, which is almost identical to the control (Conv) and very similar to the one reported previously for the same precursor [31] or other lignin-based precursors [40]. This is a clear improvement over the high-power MW carbonisation of lignin-based fibre and over the progressive MW carbonisation of PAN fibre. The main reason for this remarkable result is undoubtedly the reduction of heating rates during the initial carbonisation stage, especially in the range of 400–800 °C which allows more time for carbonisation reactions, and slower evolution of volatile products, and this improves morphology of the carbon phase. This is achieved more easily in MW carbonisation of lignin-based precursor, most likely due to larger diameter (almost an order of magnitude compared to PAN) and the resulting lower MW susceptor to fibre volume ratio which allows fibres retain their overall shape.

Mechanical properties of CFs produced via progressive MW carbonisation from lignin-based precursor are shown in Fig. 5D. Properties are compared to conventional carbonisation (Conv) at 1000, 1400, 1600 and 2000 °C. Average TS, YM and strain of samples coated before stabilisation are in the range of 0.13–0.31 GPa, 51–81 GPa and 0.23–0.5%, respectively. Average TS, YM and strain of samples coated after stabilisation are in the range of 0.08–0.33 GPa, 34.67–64.67 GPa and 0.21–0.57%, respectively. TS of fibres carbonised in MW exceeded the performance of  $0.25 \pm 0.05$  GPa for conventional carbonisation (Conv) at 1000 °C. Even a single layer of susceptor (1c) is sufficient to produce CFs in MW which are comparable with this result. Furthermore, most of the values overlap with the result of  $0.36 \pm 0.06$  GPa for conventional carbonisation (Conv) at 1400 °C, with the

**Fig. 6** Experimental vs. modelled MW heating profiles at 2.45 GHz, 700 W. Experimental PAN 1–5c (A), model for diameter 10  $\mu\text{m}$  and susceptor thickness corresponding to 1–5c (B)



closest values reported for 5 cycles of susceptor coating. This improvement can be attributed to the reduction of heating rates and temperatures during the initial heating stage and is in good agreement with the improved morphology revealed by SEM. Similarly, mechanical properties of CFs produced in microwave-assisted plasma were improved by the addition of low-temperature pre-carbonisation step [41]. Values of YM match those of samples carbonised conventionally (Conv) at temperatures of 1400  $^{\circ}\text{C}$  or higher, which implies that an improvement of the YM could be achieved by optimisation of MW carbonisation through power, time or temperature variation. Strain at failure averaged at values of conventional carbonisation at 1400–1600  $^{\circ}\text{C}$  and in some cases was found superior to sample Conv. carbonised at 2000  $^{\circ}\text{C}$ .

This is an excellent result illustrating that, if proper conditions are used, susceptor-assisted MW carbonisation proposed in this work can be successfully applied for rapid carbonisation of CFs with mechanical performance comparable with conventional carbonisation. Reduction of high heating rates observed during intermediate stages of MW carbonisation will eliminate pores from all cross-sections. This will improve the reliability of the process and increase the average mechanical properties. Further improvement of mechanical performance of the presented lignin-based CFs could be achieved by reduction of fibre diameter [24, 27, 31], as illustrated by reported TS of  $1.1 \pm 0.1$  GPa for the same precursor with a final diameter of  $25 \pm 3$   $\mu\text{m}$ . On the other hand, this will require closer control of susceptor coating thickness, MW power and other process conditions in order to tune MW heating.

Carbonisation conditions and properties of CFs produced via progressive MW carbonisation from lignin/TPU precursor are summarised in Table S5 and compared to conventional carbonisation at 1000, 1400, 1600 and 2000  $^{\circ}\text{C}$ . Conversion rate evaluated from TGA is in the range of 91.9–94.4% for fibres coated before stabilisation and 78.8–98.6% for fibres coated after stabilisation (Fig. S7). Significant improvement in conversion over full-power carbonisation can be explained by the smaller diameter of

PF and is in agreement with  $T_{\text{max}}$  temperatures  $>1000$   $^{\circ}\text{C}$  recorded for all samples. Highest conversion rates are observed for coating after stabilisation, which is in good agreement with previous findings. The calculated graphitic crystallite size ( $L_a$ ) from the Raman spectra shown in Fig. S13 is in the range of 5.12–7.12 nm for CFs coated before stabilisation, 5.02–6.73 nm for CFs coated after stabilisation and 6.71 nm for conventional carbonisation at 1000  $^{\circ}\text{C}$ . This is an improvement over high-power carbonisation and is in agreement with the general trends observed for  $T_{\text{max}}$ . Calculated values are higher than  $L_a$  size reported for the same precursor, but this is due to different calculation methods being employed [31].

Experimental and modelled MW heating profiles are compared in Fig. 6. Experimental MW heating of PAN samples 1–5c is compared to modelled MW heating using corresponding susceptor thickness. It is observed that modelled rates are two orders of magnitude higher from experimental heating rates and that modelled maximum temperatures ( $T_{\text{max}}$ ) (1020–1320  $^{\circ}\text{C}$ ) are similar than those recorded experimentally (910–1060  $^{\circ}\text{C}$ ). In addition, the model represents the trend observed experimentally according to the coating thickness. More coating cycles increase the susceptor coating that is translated into higher temperature profiles, which is exactly what is predicted in the model. The differences in the heating rates are mainly attributed to the assumption that the susceptor coating is entirely composed of MWCNTs (which is not true because the MWCNTs have some voids between them and are covered by the stabilisers) and that no heat transfer occurs within the coating itself. The peak intensity of the electric field is expected to act on each fibre in the bundle. None of the reactions taking place during the conversion of PF to CF are taken into account in the model, and this leads to predicted heating rates which are higher and the absence of peaks/disruptions, as seen in the experimental data. The modelled heat loss is a function of an assumed value for emissivity ( $\epsilon$ ).

As the carbon phase develops within the fibre, it changes from MW transparent to MW absorbing. This increases its contribution to heat generation.

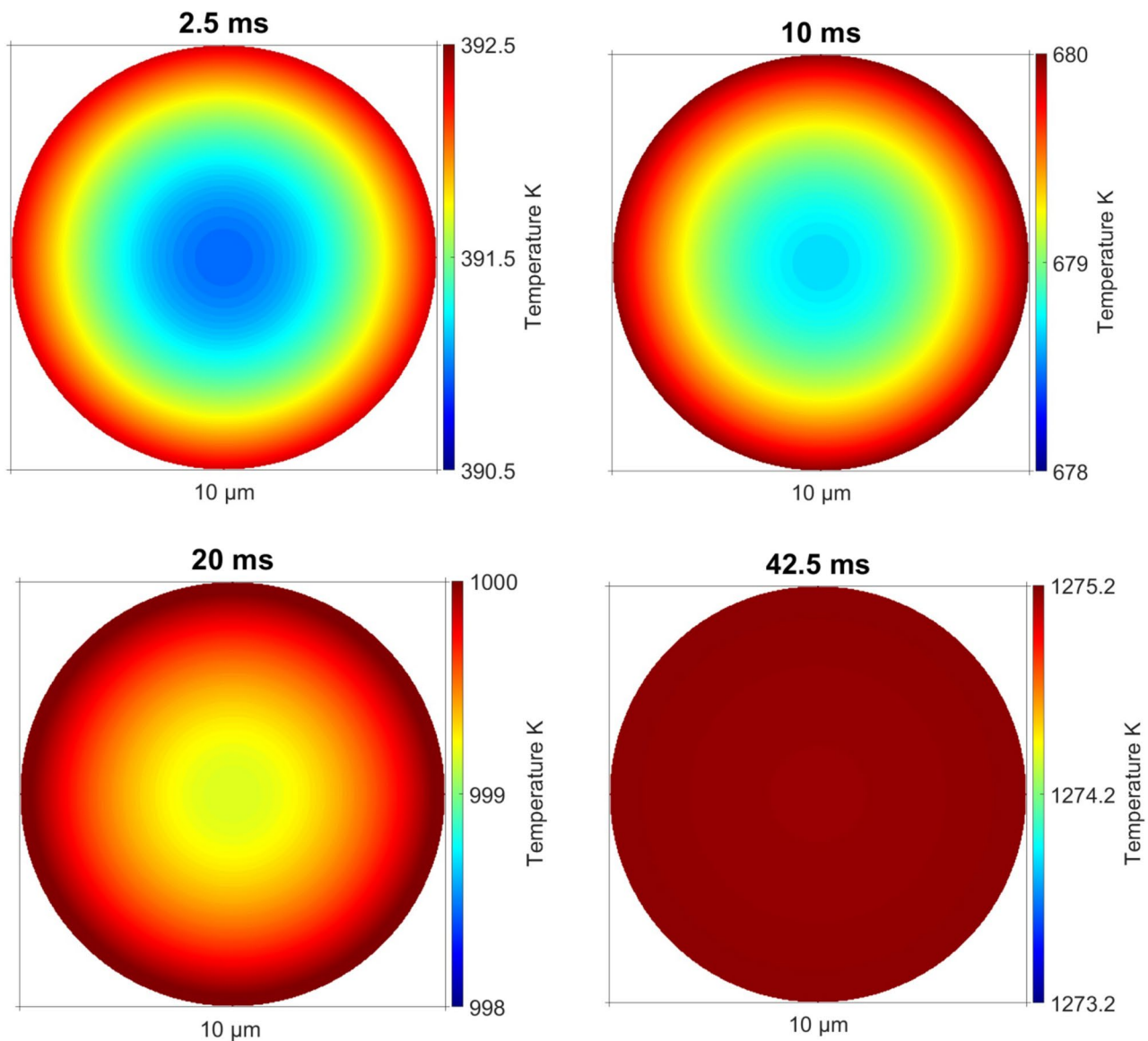


**Fig. 7** Modelled cross-section of PF (10  $\mu\text{m}$  diameter and 100 nm susceptor coating) showing edge-to-core temperature distribution at 2.5, 10, 20 and 42.5 ms of MW heating, which correspond to fibre temperatures of approximately 100, 400, 700 and 1000  $^{\circ}\text{C}$ , respectively

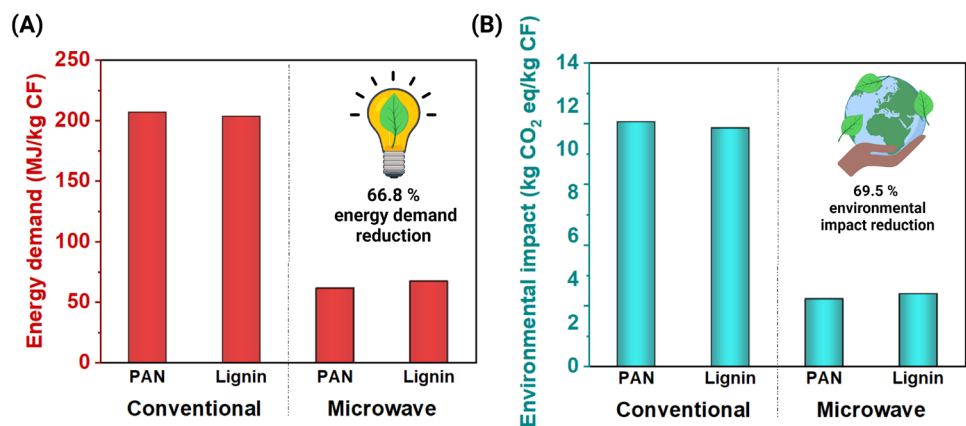
A  $T_{\text{max}}$  closest to experimental data is obtained for a modelled susceptor thickness of about 100 nm. This is therefore used for modelling temperature gradients within the PF cross-section. The modelled results for a 10  $\mu\text{m}$  diameter PF cross-section heated via a 100 nm layer of the susceptor in an electromagnetic field of a microwave are shown in Fig. 7. Four points in time are chosen to visualise temperature distributions at 100, 400, 700 and 1000  $^{\circ}\text{C}$ . A maximum edge-to-core temperature difference of 1.5  $^{\circ}\text{C}$  is observed at the start of heating, and this decreases over time of 43 ms to a difference of 0.02  $^{\circ}\text{C}$  at 1000  $^{\circ}\text{C}$ . At this point, fibre reaches a stable  $T_{\text{max}}$ , as shown in Fig. 6B.

Increasing the precursor diameter to 70  $\mu\text{m}$  decreases the rate of MW heating (Fig. S1). In this case, the edge-to-core

difference at the start of the heating reaches nearly 9.9  $^{\circ}\text{C}$  and decreases over time of 295 ms to a difference of 0.17  $^{\circ}\text{C}$  at 1000  $^{\circ}\text{C}$ . This confirms that increases in diameter result in larger temperature gradients during heating. Interestingly, a predicted  $T_{\text{max}}$  close to 1000  $^{\circ}\text{C}$  is observed regardless of the fibre diameter. The model does not take into account the absorption of MWs by the precursor material itself, and therefore, the modelled diameter has little effect once the temperature reaches the maximum where the equilibrium between the heat generated in the susceptor and the heat lost through radiation/convection is achieved.

Life cycle analysis of MW heating was performed to quantify the environmental and cost benefits achieved via MW carbonisation (the LCA methodology is described in

**Fig. 8** **A** Energy demand and **B** environmental impact for production of 1 kg of CFs using different carbonisation techniques (conventional vs. microwave) and precursor materials (PAN vs. lignin/TPU)



the SI file). The energy demand and environmental impact for the production of 1 kg of CF from PAN and lignin-based precursor via conventional and MW heating are compared in Fig. 8.

Using MW technology for CF production shows great potential to decrease the cumulative energy demand for both PAN and lignin-based fibres. It is predicted that the application of MW heating reduces the energy demand of PAN-based and lignin blend-based CF production by 70.2% and 66.8% respectively. Results also show that the climate impact of the CFs production using a conventional furnace is significantly higher for PAN-based fibres compared to lignin-based fibres, despite the lower carbon yield of the latter material. This is attributed to the lower climate impact of PF production. Furthermore, lignin's inherent properties in theory reduce the energy consumption in the CF production step due to the high level of aromaticity [42]. MW technology also reduces the CO<sub>2</sub> emission of PAN-based CF production to 27.6% of its conventional process value. Application of a lignin blend reduces the climate impact of PF production by up to 69.5%. This MW technique is a breakthrough in the field of composite materials and holds the potential for integration into various other advanced applications that typically rely on conventional carbonisation processes [43–49].

## 4 Conclusions

The results indicate that CFs can be produced from different precursors (PAN and lignin) that do not absorb MW energy (Fig. S14) via susceptor-induced MW heating with reasonable mechanical properties in comparison with conventional heating. Proposed coupled electromagnetic-heat transfer model predicts that MW heating rate and  $T_{\max}$  increase with increasing thickness of susceptor (MWCNTs) and MW power. Predicted initial heating rate is inversely proportional to precursor fibre diameter due to decreased

susceptor-to-fibre volume ratio. This study concludes that susceptor-assisted MW carbonisation results in rapid heating (20–40 min), with the highest recorded  $T_{\max}$  of 1346 °C, good conversion rates and  $L_a$  values comparable with the conventional carbonisation process. Addition of stages with reduced MW power results in a reduction of initial heating rates and  $T_{\max}$  temperatures. Consequently, this results in significant improvement of morphology and production of lignin-based CFs with matching or superior properties compared to conventional process in less than 40 min. Reduction of heating rates during intermediate stages of MW carbonisation (600–800 °C) is required to ensure the reliability of the process. Coating samples before stabilisation results in lower  $T_{\max}$  and consequently lower conversion rate and  $L_a$  size, compared to samples coated after stabilisation. This is most likely due to the fusion/melting of the susceptor layer during stabilisation, which results in reduced efficiency in MW absorption but produces more consistent results. Increasing the number of MW susceptor coating cycles generally improves the absorption of MWs and increases  $T_{\max}$ . Life cycle assessment predicts that MW heating reduces the energy demand and environmental impact of lignin-based CF production by up to 66.8% and 69.5%, respectively.

**Supplementary Information** The online version contains supplementary material available at <https://doi.org/10.1007/s42114-024-00853-2>.

**Acknowledgements** MAS, TJC, FH, MJ, MS, EF, MC and MNC acknowledge received funding from the Bio-Based Industries Joint Undertaking under the European Union's Horizon 2020 research and innovation programme under grant agreement No 720707. MM and MNC would like to acknowledge support from the Irish Government funding via the DAFM NXTGENWOOD research program 2019PROG704. MNC also acknowledges VIBES. VIBES is a project funded by the European Commission. This project has received funding from the Bio-Based Industries Joint Undertaking (JU) under grant agreement No 101023190. The JU receives support from the European Union's Horizon 2020 research and innovation programme and the Bio-Based Industries Consortium. This article reflects only the author's view, and the JU is not responsible for any use that may be made of the information it contains.

**Author contribution** M.A.S. conducted the experiments and wrote the main manuscript text. M.M. prepared figures and contributed to the writing. T.J.C. developed the thermal model and wrote the supplementary section. F.H., M.J. and M.S. developed the LCA model and wrote the supplementary section. E.F. wrote the main manuscript. M.C. conducted experiments and wrote the paper. M.N.C. wrote the paper and secured funding. All authors reviewed the manuscript.

**Funding** Open Access funding provided by the IReL Consortium The study received funding from Bio-Based Industries Joint Undertaking under the European Union's Horizon 2020 research and innovation programme under grant agreement No 720707.

**Data availability** The raw/processed data required to reproduce these findings cannot be shared at this time as the data also forms part of an ongoing study.

## Declarations

**Competing interests** The authors declare no competing interests.

**Open Access** This article is licensed under a Creative Commons Attribution 4.0 International License, which permits use, sharing, adaptation, distribution and reproduction in any medium or format, as long as you give appropriate credit to the original author(s) and the source, provide a link to the Creative Commons licence, and indicate if changes were made. The images or other third party material in this article are included in the article's Creative Commons licence, unless indicated otherwise in a credit line to the material. If material is not included in the article's Creative Commons licence and your intended use is not permitted by statutory regulation or exceeds the permitted use, you will need to obtain permission directly from the copyright holder. To view a copy of this licence, visit <http://creativecommons.org/licenses/by/4.0/>.

## References

- Jin F-L, Lee S-Y, Park S-J (2013) Polymer matrices for carbon fiber-reinforced polymer composites. *Carbon letters* 14(2):76–88
- Fan G et al (2021) Dielectric dispersion of copper/rutile cermets: dielectric resonance, relaxation, and plasma oscillation. *Scripta Mater* 190:1–6
- Fan G et al (2021) Doped ceramics of indium oxides for negative permittivity materials in MHz-kHz frequency regions. *J Mater Sci Technol* 61:125–131
- Xie P et al (2017) C/SiO<sub>2</sub> meta-composite: overcoming the  $\lambda/a$  relationship limitation in metamaterials. *Carbon* 125:1–8
- Majewski P et al (2022) End-of-life policy considerations for wind turbine blades. *Renew Sustain Energy Rev* 164:112538
- Egede P (2017) Chapter 2 -Electric Vehicles, Lightweight Design and Environmental Impacts in Environmental assessment of lightweight electric vehicles. Springer, pp 9–40
- Mainka H et al (2015) Lignin – an alternative precursor for sustainable and cost-effective automotive carbon fiber. *J Market Res* 4(3):283–296
- Collins MN, Culebras M, Ren G (2022) Chapter 8 - The use of lignin as a precursor for carbon fiber-reinforced composites. In: Puglia D, Santulli C, Sarasini F (eds) *Micro and Nanolignin in Aqueous Dispersions and Polymers*. Elsevier, pp 237–250
- Jędrzejczak P et al (2021) The role of lignin and lignin-based materials in sustainable construction – a comprehensive review. *Int J Biol Macromol* 187:624–650
- Beaucamp A et al (2022) Lignin for energy applications – state of the art, life cycle, technoeconomic analysis and future trends. *Green Chem* 24(21):8193–8226
- Hassan MF et al (2020) Recent trends in activated carbon fibers production from various precursors and applications—a comparative review. *J Anal Appl Pyrol* 145:104715
- Yuan G et al (2023) Boron and fluorine Co-doped laser-induced graphene towards high-performance micro-supercapacitors. *Carbon* 212:118101
- Skoda D et al (2023) Nickel nanoparticle-decorated reduced graphene oxide via one-step microwave-assisted synthesis and its lightweight and flexible composite with polystyrene-block-poly(ethylene-ran-butylene)-block-polystyrene polymer for electromagnetic wave shielding application. *Advanced Composites and Hybrid Materials* 6(3):113
- Antunes E et al (2018) Microwave pyrolysis of sewage biosolids: dielectric properties, microwave susceptor role and its impact on biochar properties. *J Anal Appl Pyrol* 129:93–100
- Haque KE (1999) Microwave energy for mineral treatment processes—a brief review. *Int J Miner Process* 57(1):1–24
- Culebras M et al (2017) High thermoelectric power factor organic thin films through combination of nanotube multilayer assembly and electrochemical polymerization. *ACS Appl Mater Interfaces* 9(7):6306–6313
- Sekii Y, Hayashi T (2009) Measurements of reflectance and thermal emissivity of a black surface created by electrostatic flocking with carbon-fiber piles. *IEEE Trans Dielectr Electr Insul* 16(3):649–654
- Wang F et al (2014) Effects of heat treatment and coatings on the infrared emissivity properties of carbon fibers. *J Mater Res* 29(10):1162–1167
- Wang C et al (2021) Temperature evolution, atomistic hot-spot effects and thermal runaway during microwave heating of polyacrylonitrile: a ReaxFF molecular dynamics simulation. *Nano Select* 2(12):2373–2379
- Tuinstra F, Koenig JL (1970) Raman spectrum of graphite. *J Chem Phys* 53(3):1126–1130
- Caçado L et al (2006) General equation for the determination of the crystallite size L[a] of nanographite by raman spectroscopy. *Appl Phys Lett* 88:163106–163106
- Wernet G et al (2016) The ecoinvent database version 3 (part I): overview and methodology. *The International Journal of Life Cycle Assessment* 21(9):1218–1230
- Jain MK, Abhiraman AS (1987) Conversion of acrylonitrile-based precursor fibres to carbon fibres. *J Mater Sci* 22(1):278–300
- Frank E et al (2014) Carbon fibers: precursor systems, processing, structure, and properties. *Angew Chem Int Ed* 53(21):5262–5298
- Knibbs RH (1971) The use of polarized light microscopy in examining the structure of carbon fibres\*. *J Microsc* 94(3):273–281
- Jin S et al (2017) Comparison of microwave and conventional heating methods in carbonization of polyacrylonitrile-based stabilized fibers at different temperature measured by an in-situ process temperature control ring. *Polym Degrad Stab* 140:32–41
- Morgan P (2005) Chapter 5 - Carbon Fiber Production using a PAN Precursor in Carbon fibers and their composites. CRC Press, pp 184–268
- Xue TJ, McKinney MA, Wilkie CA (1997) The thermal degradation of polyacrylonitrile. *Polym Degrad Stab* 58(1):193–202
- Zhao C et al (2000) Hybrid sintering with a tubular susceptor in a cylindrical single-mode microwave furnace. *Acta Mater* 48(14):3795–3801
- Schuepfer DB et al (2020) Assessing the structural properties of graphitic and non-graphitic carbons by Raman spectroscopy. *Carbon* 161:359–372
- Culebras M et al (2018) Biobased structurally compatible polymer blends based on lignin and thermoplastic elastomer

- polyurethane as carbon fiber precursors. *ACS Sustain Chem Eng* 6(7):8816–8825
32. Brodin I et al (2012) Oxidative stabilisation of kraft lignin for carbon fibre production 66(2):141–147
  33. Gellerstedt G et al (2013) A new method for stabilizing softwood kraft lignin fibers for carbon fiber production. *J Appl Polym Sci* 128:3824–3830
  34. Lü Y-G et al (1998) Skin-core structure in mesophase pitch-based carbon fibers: causes and prevention. *Carbon* 36(12):1719–1724
  35. Compere A et al (2005) Evaluation of lignin from alkaline-pulped hardwood black liquor. *ORNL* 118:6–97
  36. Luo J et al (2011) Lignin recovered from the near-neutral hemicellulose extraction process as a precursor for carbon fiber. *Bioresources* 6(4):4566–4593
  37. Fang W et al (2017) Manufacture and application of lignin-based carbon fibers (LCFs) and lignin-based carbon nanofibers (LCNFs). *Green Chem* 19(8):1794–1827
  38. Lin J et al (2010) Direct fabrication of highly nanoporous polystyrene fibers via electrospinning. *ACS Appl Mater Interfaces* 2(2):521–528
  39. Liu W, Zhao G (2012) Effect of temperature and time on microstructure and surface functional groups of activated carbon fibers prepared from liquefied wood. *BioResources* 7:5552–5567
  40. Beaucamp A et al (2019) Carbon fibres from renewable resources: the role of the lignin molecular structure in its blendability with biobased poly(ethylene terephthalate). *Green Chem* 21(18):5063–5072
  41. Kim SY et al (2015) Two step microwave plasma carbonization including low plasma power pre-carbonization for polyacrylonitrile based carbon fiber. *Polymer* 69:123–128
  42. Das S (2011) Life cycle assessment of carbon fiber-reinforced polymer composites. *Int J Life Cycle Assess* 16(3):268–282
  43. Ruan J et al (2023) High-conductivity nickel shells encapsulated wood-derived porous carbon for improved electromagnetic interference shielding. *Carbon* 213:118208
  44. Fan W et al (2023) MXene enhanced 3D needled waste denim felt for high-performance flexible supercapacitors. *Nano-Micro Letters* 16(1):36
  45. Beaucamp A et al (2024) Sustainable lignin-based carbon fibre reinforced polyamide composites: production, characterisation and life cycle analysis. *Compos Commun* 45:101782
  46. Muddasar M et al (2024) (2024) Synthesis of sustainable lignin precursors for hierarchical porous carbons and their efficient performance in energy storage applications. *ACS Sustain Chem Eng* 12(6):2352–2363
  47. Beaucamp A et al (2022) Sustainable lignin precursors for tailored porous carbon-based supercapacitor electrodes. *Int J Biol Macromol* 221:1142–1149
  48. Zeng J et al (2024) Magnetic field facilitated electrocatalytic degradation of tetracycline in wastewater by magnetic porous carbonized phthalonitrile resin. *Appl Catal B* 340:123225
  49. Kang F et al (2023) Electron-rich biochar enhanced Z-scheme heterojunctioned bismuth tungstate/bismuth oxyiodide removing tetracycline. *Inorg Chem Front* 10(20):6045–6057

**Publisher's Note** Springer Nature remains neutral with regard to jurisdictional claims in published maps and institutional affiliations.